Low Phase Noise G_m-Boosted Differential Gate-to-Source Feedback Colpitts CMOS VCO

Jong-Phil Hong, *Student Member, IEEE*, and Sang-Gug Lee, *Member, IEEE*

***Abstract*—This paper presents a g_m-boosted differential gate-to-source feedback Colpitts (GS-Colpitts) CMOS voltage-controlled oscillator (VCO) that consumes a lower oscillation start-up current. The proposed architecture allows a wider range of saturation mode operation for the switching transistors, which helps suppress AM-to-FM conversion by these transistors. In addition, the phase noise contribution of the flicker noise in the switching transistor is reduced through the capacitor feedback network of the Colpitts oscillator. As a result, the proposed topology can achieve better phase noise performance and a higher figure of merit (FOM) compared to a conventional NMOS-only cross-coupled VCO. The proposed VCO is implemented in a 0.18-μm CMOS for 1.78 to 1.93 GHz operation. At 1.86 GHz, the measurements show phase noise of -105 and -128 dBc/Hz (corresponding to $\mathrm{FOM} = 191.2$) at offsets of 100 kHz and 1 MHz, respectively, while dissipating 1.8 mA from a 0.9-V supply.**

***Index Terms*—AM-to-FM conversion, CMOS, Colpitts, phase noise, voltage controlled oscillator.**

I. Introduction

IN RESPONSE to the high-performance requirement in wireless communication applications, several types of LC-VCOs with low power, wide frequency tuning range, low phase noise, and small chip area have been developed. Among these structures, NMOS-only and complementary cross-coupled differential VCOs in a CMOS have been widely adopted owing to their ease of implementation and good phase noise performances. However, the NMOS-only topology has become popular with technology scaling due to its supply voltage reduction, (less than 1 V), whereas the complementary VCO tends to be avoided due to its voltage headroom limitation $(2\mathrm{V_{th}} + \mathrm{V_{ds}})$ caused by N- and PMOS transistor stacking. Only as recent as a few decades ago, despite their superior phase noise property, single-ended Colpitts VCOs were rarely adopted as an integrated circuit due to their non-differential output and poor start-up characteristic requiring high-power dissipation. Lately, however, several differential Colpitts structures that overcome these disadvantages through negative $\mathrm{g_m}$-boosting techniques have been reported [1]–[6]. Furthermore, the proposed $\mathrm{g_m}$-boosted differential Colpitts VCO can be used in low-supply applications since they stack only NMOS transistors.

With VCOs operating in a current-limited regime, when switching transistors enter into the triode region, the close-in ($1/f^3$ region) phase noise degradation through the AM-to-FM conversion is dominated by the effective capacitance variation of the switching transistors with a voltage swing [7]. In addition, as the switching transistors operate in triode mode, the phase noise of the $1/f^2$ region degrades due to increased switching transistor noise and reduced oscillation amplitude [5], [9]. Many techniques that prevent the switching transistors from entering the triode mode even at a large output oscillation amplitude have been reported [7]–[11]. With these techniques, in spite of the noise addition by the $\mathrm{g_m}$-boosting transistors, $\mathrm{g_m}$-boosted differential Colpitts VCOs still show a good close-in phase noise characteristic by suppressing the transistor flicker noise [2]–[4], [12]. Accordingly, $\mathrm{g_m}$-boosted differential Colpitts architectures are gaining attention as integrated VCO designs in advanced CMOS technologies where the transistor flicker noise becomes more significant.

This paper reports on a $\mathrm{g_m}$-boosted differential Colpitts VCO with gate-to-source feedback (GS-Colpitts). Section II describes the proposed GS-Colpitts VCO structure and analyzes the negative conductance and oscillation amplitude according to the $\mathrm{g_m}$-boosting factor. Section III analyzes the phase noise characteristics of the proposed topology including the capacitive division effect and compares the proposed structure with a conventional NMOS-only LC-VCO. In Section IV, the measurement results of the GS-Colpitts and conventional cross-coupled VCO are presented and compared with analysis and simulation results. In Section V summarizes the findings of this paper.

II. $\mathrm{G_m}$-Boosted Differential GS-Colpitts VCO Design

Fig. 1 shows a conventional NMOS-only crossed-coupled LC-VCO [Fig. 1(a)] and the proposed $\mathrm{g_m}$-boosted differential Colpitts VCO [Fig. 1(b)] that adopts a gate-to-source feedback network including an output buffer. In the proposed $\mathrm{g_m}$-boosted differential GS-Colpitts VCO, shown in Fig. 1(b), transistor $\mathrm{M_0}$ is the current source and $\mathrm{M_3}$–$\mathrm{M_4}$ are the $\mathrm{g_m}$-boosting transistors. In Fig. 1(b), differential operation is realized by adopting a current source $\mathrm{M_0}$, and $\mathrm{g_m}$-boosting is achieved by connecting the gates of $\mathrm{M_{3,4}}$ to the gates of opposite switching transistors $\mathrm{M_{1,2}}$ for positive feedback generation. The $\mathrm{g_m}$-boosting transistors $\mathrm{M_{3,4}}$ enhance the overall small-signal loop gain of the proposed GS-Colpitts VCO, increasing the negative conductance and reducing the start-up current. In Fig. 1(b), instead of the source, the gate terminal of $\mathrm{M_{1,2}}$ is selected for sampling of the feedback signal, which allows lower supply voltage

Manuscript received May 07, 2009; revised August 07, 2009. Current version published October 23, 2009. This paper was approved by Associate Editor Behzad Razavi. This work was supported by a Korea Science and Engineering Foundation (KOSEF) Grant (No. R0A-2007-000-10050-0) funded by the Korea government (MEST).

The authors are with the Korea Advanced Institute of Science and Technology (KAIST), Daejeon 305-701, Korea (e-mail: jongph@kaist.ac.kr; sglee@ee.kaist.ac.kr).

Color versions of one or more of the figures in this paper are available online at http://ieeexplore.ieee.org.

Digital Object Identifier 10.1109/JSSC.2009.2031519

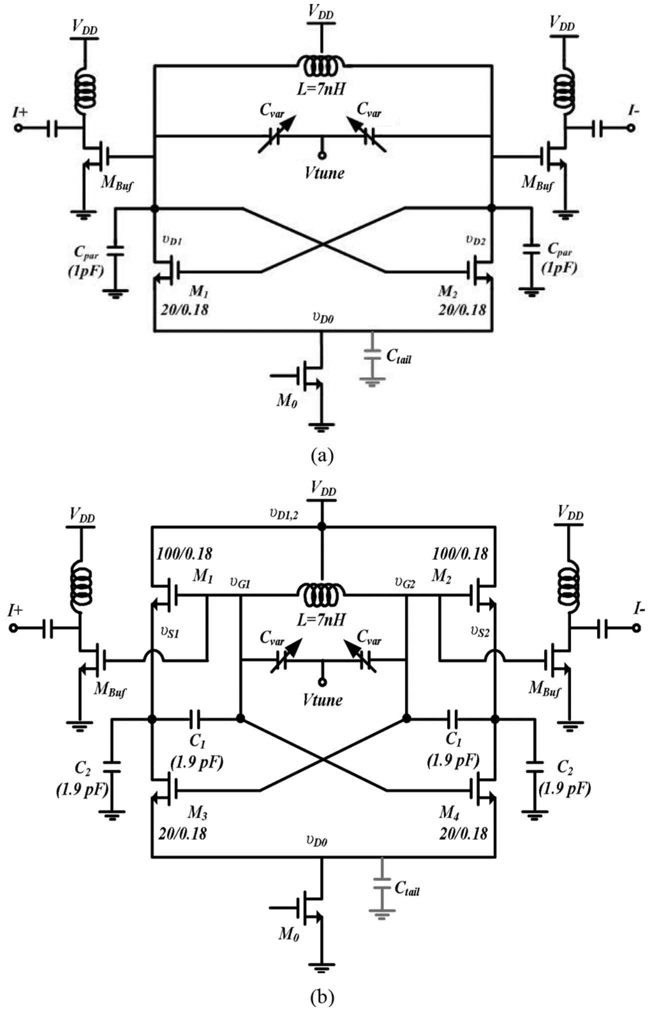

Fig. 1. VCO schematics including output buffer for the (a) conventional NMOS-only cross-coupled and (b) proposed $\mathrm{g_m}$-boosted differential GS-Colpitts.

operation. In order to start oscillation, the transistors ($\mathrm{M}_{1,2}$, $\mathrm{M}_{3,4}$, and M_0) must be biased in the saturation region. Due to the additional NMOS $\mathrm{g_m}$-boosting transistor $(\mathrm{M}_{3,4})$ staking, the proposed $\mathrm{g_m}$-boosted GS-Colpitts oscillator requires higher $(\mathrm{V_{DS3,4}})$ supply voltage compared to that of the conventional NMOS-only VCO. This decreases the overdrive voltage of the tail current source transistor in the proposed VCO. However, the minimum supply voltage of the proposed VCO is lower $(\mathrm{V_{GS1,2}}\text{–}\mathrm{V_{DS3,4}})$ than that of the complementary cross-coupled VCO.

Fig. 2 shows a circuit representation of the proposed GS-Colpitts VCO and the corresponding small-signal equivalent circuit used to estimate the negative input impedance [13]. From Fig. 2(b), where channel-length modulation and body effects are neglected

$$\begin{aligned} Y_{IN-GS} = \frac{I_x}{V_x} &= -\frac{g_{m1}\omega^2 C_1 C_2}{g_{m1}^2 + \omega^2 (C_1 + C_2)^2} \\ &\quad \cdot \frac{1}{2}\left[1 + \frac{g_{m3}}{g_{m1}}\left(1 + \frac{C_1}{C_2}\right)\right] \\ &\quad + j\frac{1}{2}\frac{\omega^3 C_1 C_2 (C_1 + C_2) - g_{m1} g_{m3} \omega C_1}{g_{m1}^2 + \omega^2 (C_1 + C_2)^2} \end{aligned} \tag{1}$$

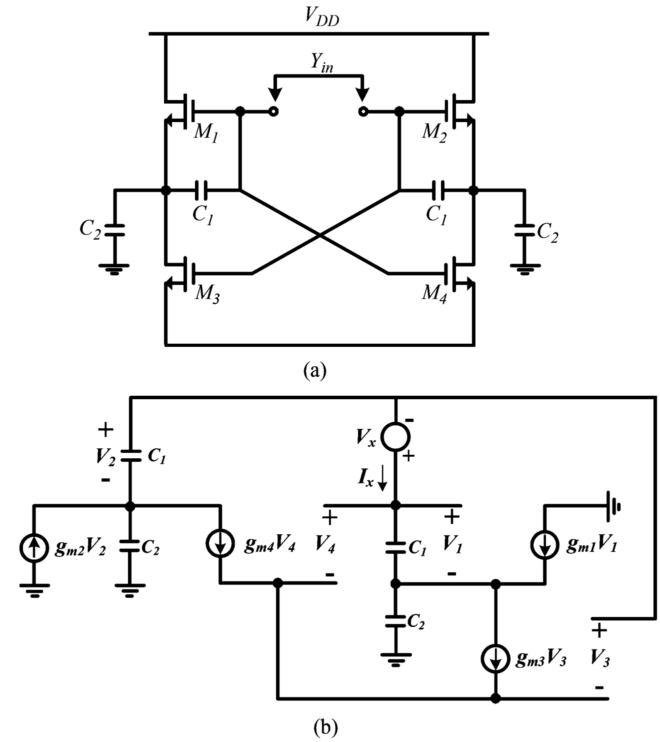

Fig. 2. (a) Proposed topology to create negative input impedance, and (b) a small signal equivalent circuit of (a) to calculate the input impedance.

where g_{m1} and g_{m3} are the transconductances of switching transistor $\mathrm{M}_{1,2}$ and $\mathrm{g_m}$-boosting transistor $\mathrm{M}_{3,4}$, respectively. Likewise, the small-signal negative conductance of the conventional GS-Colpitts oscillator [13] is given by

$$\mathrm{Re}[Y_{IN-CONV}] = -\frac{g_{m1}\omega^2 C_1 C_2}{g_{m1}^2 + \omega^2 (C_1 + C_2)^2}. \tag{2}$$

From (1) and (2), the negative conductance of the proposed $\mathrm{g_m}$-boosted GS-Colpitts VCO is increased by a factor of $0.5[1 + (g_{m3}/g_{m1})(1 + \mathrm{C}_1/\mathrm{C}_2)]$ compared to that of the conventional GS-Colpitts VCO. Therefore, the start-up current of the proposed $\mathrm{g_m}$-boosted GS-Colpitts VCO can be reduced.

To understand and estimate the oscillation amplitude of the proposed GS-Colpitts oscillator, a comparison with conventional differential Colpitts and cross-coupled oscillators, is presented in Fig. 3, where $L_{P,L} = L_{P,R}$. Figs. 3(a) and 3(b) show the operational behavior of the conventional differential GS-Colpitts and proposed $\mathrm{g_m}$-boosted GS-Colpitts oscillators, respectively. In Fig. 3(a), the conventional GS-Colpitts oscillator operates differentially by coupling of the center-tapped inductor and the gray/black parts show the off/on states of the circuits during the first half of an oscillation cycle. Fig. 3(c) represents the describing function model of Fig. 3(a) employed to calculate the oscillation amplitude [19]. In Fig. 3(a), $1/G_{m1}$ in parallel connection with C_1 represents the large-signal source-gate resistance of the transistor M_1. The large-signal transconductance G_{m1} of the transistor M_1 is given by

$$G_{m1} \approx \frac{I_1}{v_{GS} - V_{th}} \approx \frac{I_1}{(1-n)A_{tank}} \tag{3}$$

where $n \equiv \mathrm{C}_1/(\mathrm{C}_1+\mathrm{C}_2)$ is the capacitive voltage divide factor. From Fig. 3(c), the peak amplitude (A_{tank1}) of the tank voltage at resonance, during the first half, can be given by

$$\begin{aligned} A_{tank1} &\approx I_1 \cdot R_{eq} \\ &= I_1 \left(R_p \| \frac{1}{(1-n)^2 G_{m1}} \right) \\ &= I_1 \left(\frac{R_p}{(1-n)^2 G_{m1} R_p + 1} \right) \\ &= n I_1 R_p \end{aligned} \tag{4}$$

where the equivalent resistance R_{eq} represents the parallel combination of the tank resistance R_P and the transformed resistance of $1/G_{m1}[= 1/(1-n)^2 G_{m1}]$

$$R_{eq} \approx R_p \| \frac{1}{(1-n)^2 G_{m1}}. \tag{5}$$

Considering class-C operation of the Colpitts oscillator (which can also be adopted in the GS-Colpitts oscillator) [12], A_{tank} of (3) simplifies to

$$A_{tank} = n(2I_B)R_p. \tag{6}$$

During the second half, while M_1 is turned-off, the same voltage swing is induced across the same inductor $L_{P,L}$ with opposite polarity through inductive coupling from $L_{P,R}$, leading to a symmetric voltage swing. In the proposed GS-Colpitts oscillator shown in Fig. 3(b), the switching transistors $\mathrm{M}_{1,2}$ and $\mathrm{g_m}$-boosting transistors $\mathrm{M}_{3,4}$ operate in a complementary manner. As can be seen in Fig. 3(b), when the transistor $\mathrm{M}_1/\mathrm{M}_4$ turns on, the transistor $\mathrm{M}_2/\mathrm{M}_3$ turns off, and thus the voltage swing across $L_{P,L}$ is determined by the sum of the Colpitts and cross-coupled oscillator operation. Assuming the magnetic coupling coefficient k is approximately equal to 1, the peak current $(I_1 + I_2)$ induced onto the inductor $L_{P,L}$ by the cross-coupled [12] and Colpitts [19] oscillator operation is equal to $(1 + 2/\pi)(2I_B)$. Therefore, from (4), the peak amplitude of the proposed $\mathrm{g_m}$-boosted GS-Colpitts oscillator is given by

$$A_{tank} = n \left(1 + \frac{2}{\pi} \right) (2I_B) R_p. \tag{7}$$

Note that the peak amplitude of the conventional cross-coupled oscillator is given by [12]

$$A_{tank} = \frac{2}{\pi} (2I_B) R_p. \tag{8}$$

From (6) and (7), the proposed $\mathrm{g_m}$-boosted Colpitts oscillator shows more than 60% improvement in oscillation amplitude compared to that of the conventional differential GS-Colpitts oscillator. Meanwhile, from (7) and (8), for $n = 0.4$, the oscillation amplitude of the proposed $\mathrm{g_m}$-boosted GS-Colpitts oscillator becomes equal to that of the conventional cross-coupled oscillator.

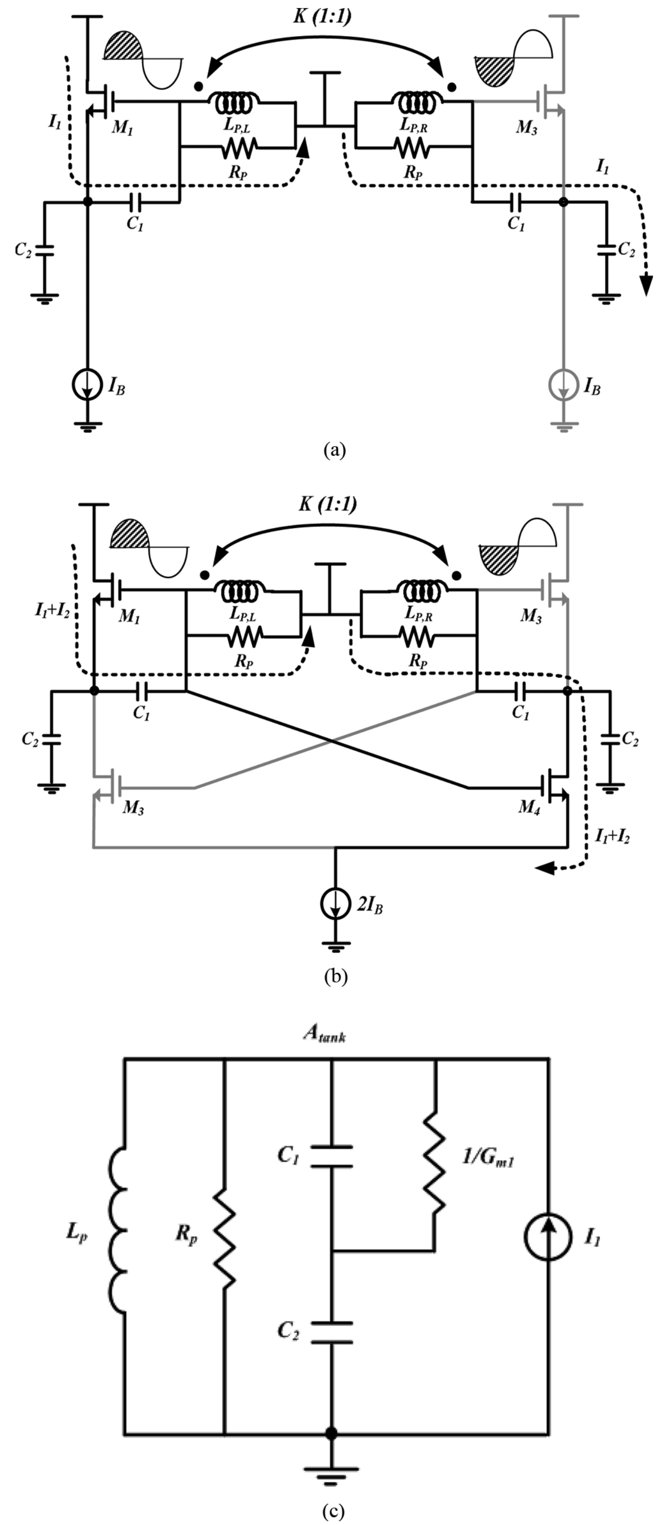

Fig. 3. Operation behavior of (a) conventional differential GS-Colpitts and (b) proposed $\mathrm{g_m}$-boosted GS-Colpitts, and (c) describing function model of (a).

Fig. 4 shows the simulated output (single) oscillation amplitude of the conventional differential GS-Colpitts, the proposed $\mathrm{g_m}$-boosted differential GS-Colpitts with $n = 0.5$ [Fig. 1(b)], and the cross-coupled LC-VCO [Fig. 1(a)], each under the same frequency of oscillation, tuning range, and quality factor of the *LC* resonator, the details of which are explained in Section III-A. As can be seen from Fig. 4, the oscillation

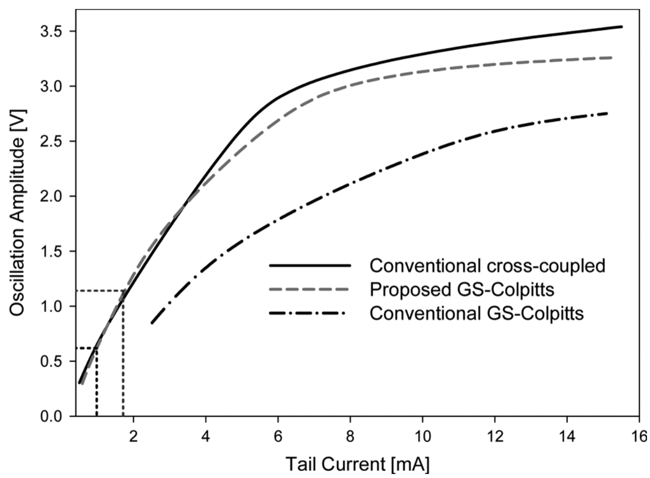

Fig. 4. Simulated output oscillation amplitude versus tail bias current at a 1.8-V supply.

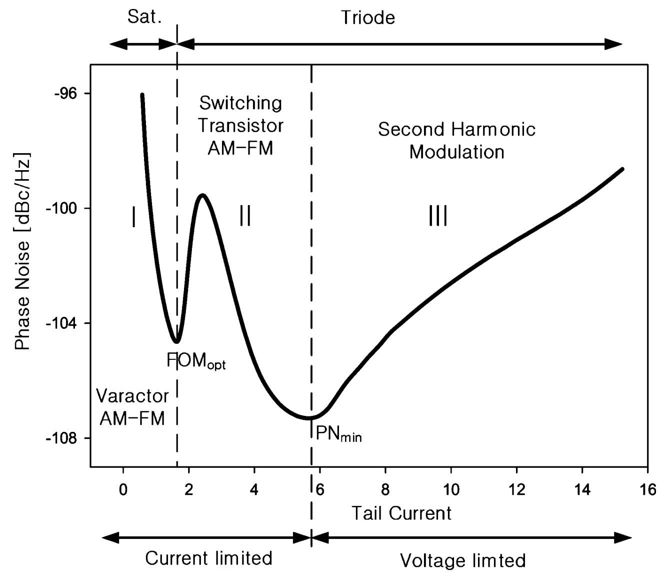

Fig. 5. Close-in phase noise behavior of the conventional VCO as a function of the tail current.

amplitudes of the three oscillators show good agreement with the results of the previous analysis. Note that, contrary to the drain-to-source feedback Colpitts oscillator, where the oscillation amplitude shows proportional dependence on $(1 - n)$, the proposed $\mathrm{g_m}$-boosted GS-Colpitts oscillator shows proportional dependence on n. That is, in the proposed $\mathrm{g_m}$-boosted GS-Colpitts oscillator, the oscillation amplitude increases as the $\mathrm{C_1/C_2}$ ratio increases.

III. Phase Noise Analysis of the Proposed GS-Colpitts VCO

In a conventional cross-coupled LC-VCO, the close-in phase noise mainly results from flicker noise of the tail current source and switching transistors. The flicker noise of the tail current source transistor ($\mathrm{M_0}$ in Fig. 1) up-converts into close-in phase noise through the AM-to-FM and CMM-to-FM conversion mechanisms. The variations in output voltage swing and common mode (CM) voltage of the varactor give rise to a change in oscillation frequency and therefore increase the phase noise [7], [14], [15]. On the other hand, the flicker noise of the switching transistors $(\mathrm{M_{1,2}}, \mathrm{M_{3,4}})$ modulates the second harmonic current at the common-source node and increases the close-in phase noise by the mixing operation through the switching transistors [16]–[18].

Fig. 5 shows the simulated close-in phase noise (100 kHz offset) of the conventional NMOS-only cross-coupled differential LC-VCO as a function of the tail current, shown in Fig. 1(a). The simulated phase noise is measured at 1.88 GHz and the component size details are also given in Fig. 1(a). The mechanisms that determine the phase noise behavior of CMOS VCO have been described in various prior works [7], [14], [17]. In Fig. 5, the ups and downs of the phase noise behavior as a function of tail current are determined by various mechanisms which will be explained later in more detail. Fig. 5 is useful as it demonstrates the optimum figure of merit $(\mathrm{FOM_{opt}})$ and minimum phase noise $(\mathrm{PN_{min}})$ points which can be used as a valuable design guideline.

In Fig. 5, the close-in phase noise behavior with respect to the tail current can be divided into three regions by the dominating mechanisms. In region I, the VCO operates under current limited mode, and the switching transistors switch between cut-off and saturation mode operations. In this region, the flicker noise of the tail current transistor is the dominant source for close-in phase noise degradation through the AM-to-FM conversion by the varactors. To minimize this effect, the VCOs are designed with a small VCO gain $(\mathrm{K_{VCO}})$ and maximize the output amplitude at the same bias current [14]. In region II, where the switching transistors circulate cut-off, saturation and triode mode operation while the VCO still operates under current limited mode, the AM-to-FM conversion by the nonlinearity, with regards to the output swing, of the parasitic capacitance of the switching transistors becomes a dominant source of close-in phase noise degradation. These nonlinear parasitic capacitor effects can be suppressed by preventing the switching transistor operation into the triode mode even at a large output of oscillation amplitude [7], [11]. In regions I and II, $1/f$ noise of the tail current transistor dominates the close-in phase noise performance compared to that of the switching transistors. However, in region III, $1/f$ noise of the switching transistor is the main source of increased close-in phase noise caused by the second harmonic modulation mechanism. This second harmonic modulation effect can be reduced by providing high impedance at the common source node of the switching transistors [18]. In the following, the phase noise behavior in region II is explained for the case of a conventional NMOS-only VCO. The details of how the dominant mechanisms in regions II and III are suppressed in the proposed GS-Colpitts VCO are also discussed below.

A. AM-to-FM Conversion by the Switching Transistors in Region II

Fig. 6 illustrates the phase noise behavior in region II of Fig. 5. Fig. 6(a) shows the cross-coupled VCO schematic excluding the LC-tank part, Fig. 6(b) the equivalent capacitance seen by the LC-tank, and Fig. 6(c) presents the time-averaged effective capacitance and the derivative seen by the LC-tank with respect to the tail current. The time-averaged effective capacitance shown in Fig. 6(c) is obtained by reverse estimation of the simulated oscillation frequency at the varactor null point [14] where the effective varactor capacitance shows no output swing dependence. From Fig. 6(b), the effective capacitance seen by the LC-tank, C_{eff}, can be expressed as a function of the output voltage swing. For small, medium, and large output voltage swings, where the switching transistors (M_1 and M_2) operation involves saturation only, saturation/cut-off, and saturation/cut-off/triode mode, respectively, the effective capacitances C_{eff1}, C_{eff2}, and C_{eff3} are given by

$$C_{eff1} = \frac{C_{gs2,sat} \cdot C_{gs1,sat}}{C_{gs2,sat} + C_{gs1,sat}} + \frac{C_{par}}{2} + C_{gd1,sat} + C_{gd2,sat} \tag{9}$$

$$C_{eff2} = \frac{C_{gs2,sat} \cdot C_{gs1,off}}{C_{gs2,sat} + C_{gs1,off}} + \frac{C_{par}}{2} + C_{gd1,off} + C_{gd2,sat} \tag{10}$$

$$C_{eff3} = \frac{C_{gs2,triode} \cdot C_{gs1,off}}{C_{gs2,triode} + C_{gs1,off}} + \frac{C_{par}}{2} + C_{gd1,off} + C_{gd2,triode} \tag{11}$$

respectively, where $C_{gs1,off}$, $C_{gs1,sat}$, $C_{gs2,sat}$, $C_{gs2,triode}$, $C_{gd1,off}$, $C_{gd1,sat}$, $C_{gd2,sat}$, and $C_{gd2,triode}$ are the gate-source and gate-drain parasitic capacitances of the switching transistors $(\mathrm{M}_{1,2})$ under cut-off, saturation, and triode mode of operation, respectively. As can be seen from (9) and (10), C_{eff2} is smaller than C_{eff1} since the values of the series connected C_{gs1} changes from $C_{gs1,sat}$ to $C_{gs1,off}$. Note that $C_{gd1,sat} = C_{gd1,off}$. Meanwhile from (10) and (11), C_{eff3} is larger than C_{eff2}, mainly due to the change of $C_{gd1,sat}$ to $C_{gd1,triode}$. Therefore, the variation of the effective capacitance with respect to the output voltage swing leads to the variation of the time-averaged effective capacitance shown in Fig. 6(c). As can be seen in Fig. 6(c), the time-averaged effective capacitance increases sharply in the early part of region II, but levels off in the deeper part of region II. As the operating condition moves deeply into region II, the switching transistors operate for a longer period in triode mode, such that the time-averaged effective capacitance varies slowly. The derivative of the time-averaged shown in Fig. 6(c) indicates the oscillation frequency sensitivity with respect to the tail current. As can be seen in Fig. 6(c), since the frequency sensitivity sharply increases in the early part of region II, the flicker noise of the tail current source transistor significantly changes the oscillation frequency, this explains the sharp increase in phase noise in region II of Fig. 5. In Fig. 5, the $\mathrm{FOM_{opt}}$ can occur at higher tail current (and therefore its value is increased) if the triode mode operation of the switching transistors can be delayed with an increase in output voltage swing.

The triode mode operation of the switching transistors can be avoided by maintaining the relation $v_{\mathrm{GS}} - \mathrm{V_{TH}} \leq v_{\mathrm{DS}}$

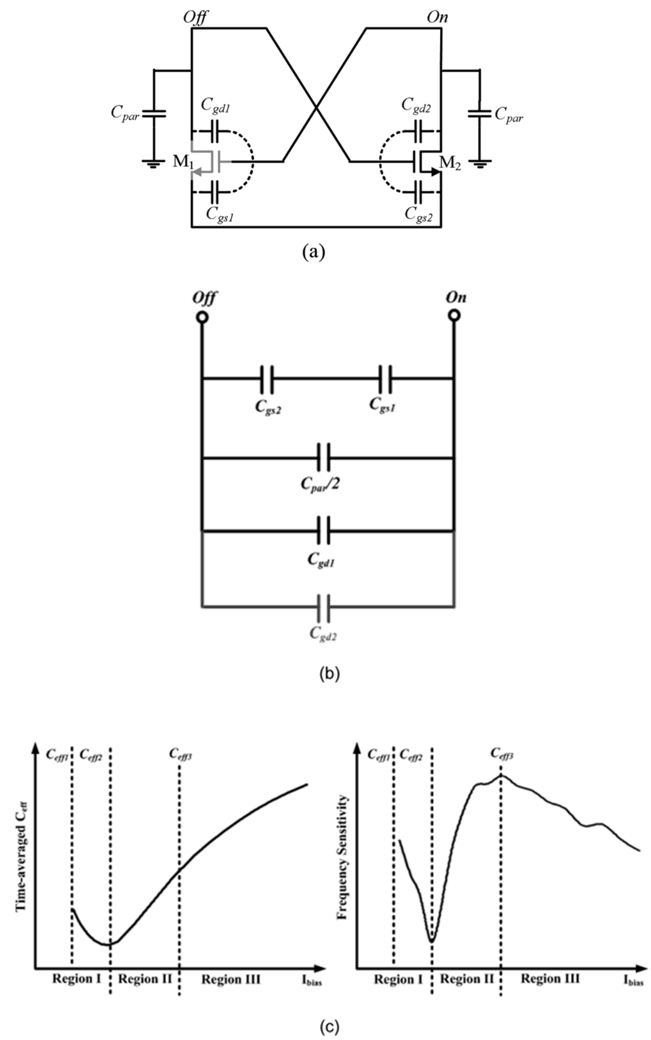

Fig. 6. (a) Cross-coupled VCO schematic excluding the LC-tank part, (b) equivalent capacitance seen by the LC-tank, and (c) time-averaged effective capacitance and the derivative seen by the LC-tank with respect to the tail current.

over the dynamic operation of the VCO. Fig. 7 shows the node voltage and branch current waveforms of the two VCOs shown in Fig. 1 with a 1.3 mA tail current. As can be seen in Fig. 7(a), with a conventional cross-coupled LC-VCO, at the point where v_{GS} is largest, v_{DS} minimizes, driving the switching transistors into triode mode. The total output voltage swing drops directly across the gate-source terminal of the switching transistors. For the proposed GS-Colpitts VCO shown in Fig. 7(b), the dynamic output voltage swing at the gate of $\mathrm{M}_{1,2}$ is divided between C_1 and C_2, leading to a smaller drop in the gate-source voltage v_{GS}' drop. Furthermore, the gate-drain voltage v_{DS}' of the switching transistors $(\mathrm{M}_{1,2})$ at the peak gate-source voltage is larger in the proposed GS-Colpitts VCO, since the drain voltage is fixed at $\mathrm{V_{DD}}$ and the source voltage is half of the drain voltage of the conventional NMOS-only VCO. Therefore, with an increase in the output voltage swing, the switching transistors $(\mathrm{M}_{1,2})$ of the proposed GS-Colpitts VCO remain in saturation mode for larger output oscillation amplitude compared to that of the conventional NMOS-only cross-coupled VCO. If the source bias

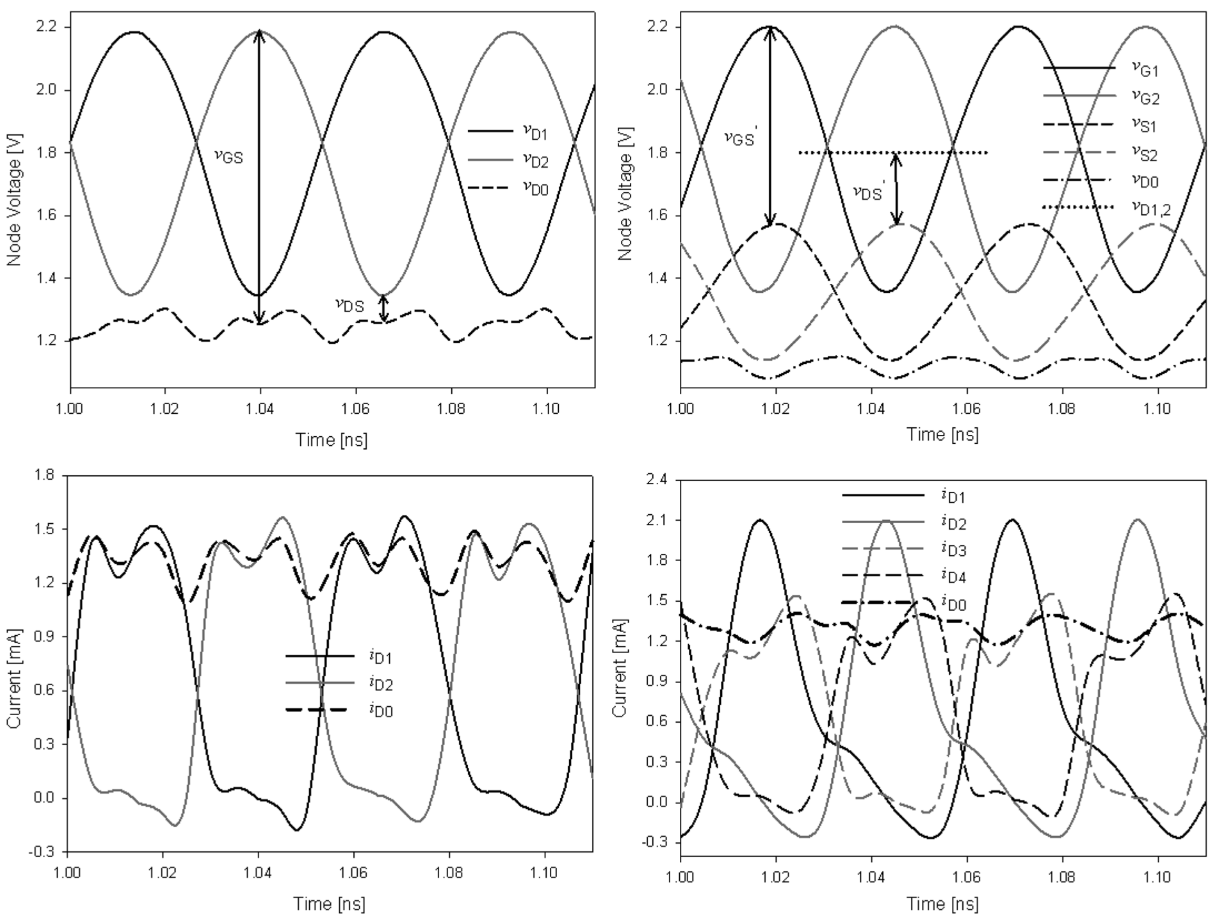

Fig. 7. Simulated node voltage and branch current behaviors of the (a) conventional cross-coupled and (b) g_m-boosted differential GS-Colpitts VCOs.

voltage V_S is the same in the two VCOs, the output oscillation amplitude (V_{TH}) of the proposed GS-Colpitts VCO can be double that $(V_{TH}/2)$ of the conventional VCO at the maximum saturation mode operation, since the drain voltage v_D is fixed at V_{DD}. In the proposed GS-Colpitts VCO, the output oscillation amplitude at the maximum saturation operation can be different due to the feedback capacitor ratio between C_1 and C_2, which will be discussed in detail in Section III-C.

The two VCOs shown in Fig. 1 are designed to oscillate from 1.78 to 1.98 GHz with a 1.8-V supply using the same value of varactors and center-tapped inductors. In the conventional VCO shown in Fig. 1(a), the size of the parallel capacitor C_{par} is chosen to have the same frequency tuning range and K_{VCO} as the proposed VCO in Fig. 1(b). Fig. 8 shows the oscillation frequency variation [Fig. 8(a)] and the absolute value of the frequency deviation [Fig. 8(b)] versus the tail current at the center frequency for the two VCOs. The oscillation frequency of the proposed GS-Colpitts and conventional VCO change abruptly at tail currents of 1.8 mA and 0.9 mA, respectively, where the switching transistors $(M_{1,2})$ start to enter triode mode operation. As can be seen in Fig. 8(b), since the maximum frequency deviation of the proposed GS-Colpitts VCO is nearly half that of the conventional VCO, the sensitivity of the oscillation frequency to the oscillation amplitude variation is reduced by half compared to that of the conventional VCO. As a result, compared to the conventional VCO, the AM-to-FM conversion by the switching transistors in the proposed GS-Colpitts VCO is delayed and suppressed, thereby yielding improved close-in phase noise.

In the proposed Colpitts VCO, the gate voltage of the switching $(M_{1,2})$ and g_m-boosting $(M_{3,4})$ transistors is the same while the drain voltage of the $M_{3,4}$ is smaller than that of $M_{1,2}$ due to the capacitive voltage division by the feedback capacitor. As a result, the g_m-boosting transistors $(M_{3,4})$ enter the triode region earlier, where the effective capacitance of the g_m-boosting transistors increases with an increase in the tail current (see Fig. 6). However, since the switching transistors $M_{1,2}$ still operate in the saturation/cut-off region, their effective capacitance decreases with an increase in tail current. Therefore, the sum of the effective capacitances provided by the switching and g_m-boosting transistors remains nearly constant with an increase in tail current, such that the AM-to-FM conversion is suppressed in this region.

Fig. 9 shows the simulation results of the phase noise versus tail bias current for the two VCOs at offset frequencies of 100 kHz and 1 MHz. The simulations are conducted at a center frequency of 1.88-GHz where the AM-to-FM conversion by the varactors is negligible. When the switching transistors $(M_{1,2})$ start entering the triode region, the close-in phase noise rapidly degrades at tail currents of 0.9 and 1.8 mA for the conven-

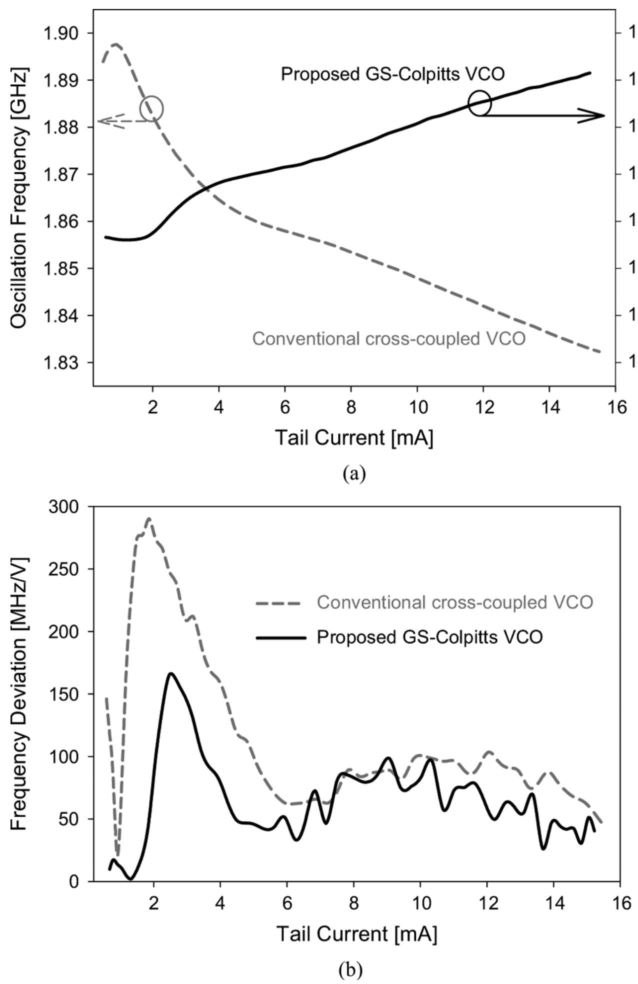

Fig. 8. Simulated (a) oscillation frequency and (b) absolute value of the frequency deviation versus tail current at the center frequency in the conventional cross-coupled (dashed-dark gray) and $\mathrm{g_m}$-boosted differential GS-Colpitts VCOs (solid-black).

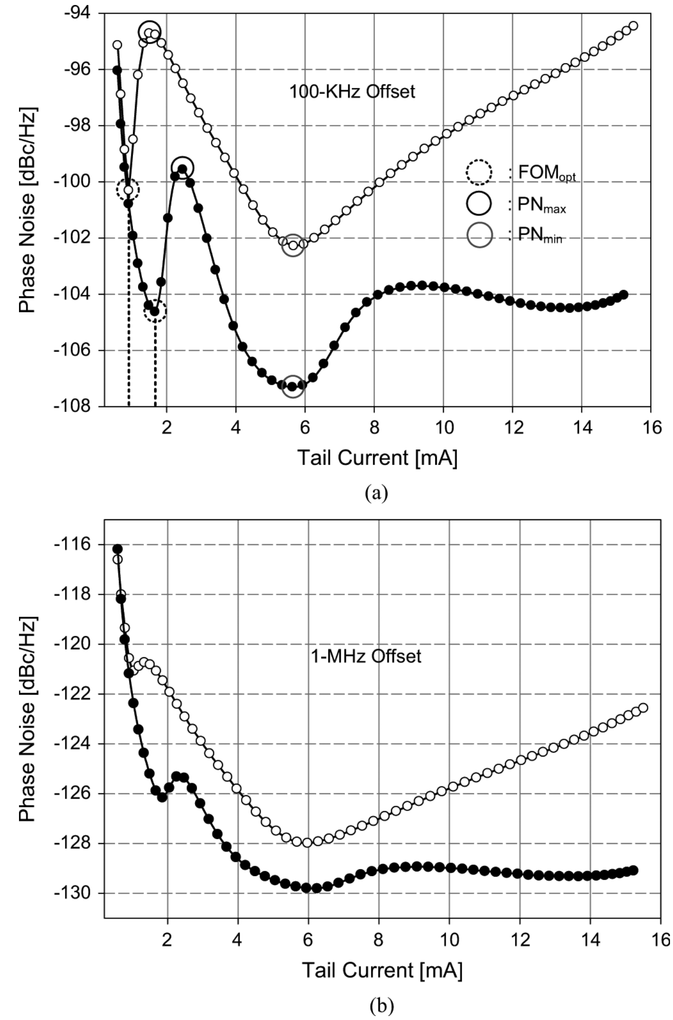

Fig. 9. Simulated phase noise at (a) 100 kHz and (b) 1 MHz offsets versus tail current in the conventional cross-coupled (white filled-circle) and $\mathrm{g_m}$-boosted differential GS-Colpitts (black filled-circle) VCOs.

tional and proposed VCOs, respectively, since the frequency sensitivity to AM-to-FM conversion by the switching transistors $(\mathrm{M_{1,2}})$ significantly increases, as shown in Fig. 8. It can be seen in Fig. 9 that the AM-to-FM conversion by switching transistors $(\mathrm{M_{1,2}})$ is the major source of phase noise degradation at region II in the two VCOs, while the AM-to-FM conversion by the switching transistors in the proposed GS-Colpitts VCO occurs at a higher tail bias current compared to the conventional VCO. In the proposed GS-Colpitts VCO, since the output oscillation amplitude (1.2 V) at the maximum saturation mode operation is twice that (0.6 V) of the conventional cross-coupled VCO, as shown in Fig. 4, and the maximum sensitivity is half, as shown in Fig. 8, the optimum $(\mathrm{FOM_{opt}})$, minimum $(\mathrm{PN_{min}})$, and maximum $(\mathrm{PN_{max}})$ phase noise in region II of the proposed GS-Colpitts VCO improve by 5 dB, respectively, compared to those of the conventional VCO as shown in Fig. 9(a). As the switching transistors enter triode mode operation, with an increase in the tail current, the increase of oscillation amplitude becomes less steep while the thermal noise increases. This mitigates the phase noise improvement ratio with respect to the increase in tail current [5]. [9]. Therefore, as can be seen in Fig. 9(b), the delay of the switching transistor operation into the triode mode at higher tail current also improves the phase noise at the $1/\mathrm{f}^2$ region (1 MHz offset). Based on Lesson's phase noise formula, a twofold increase in the output amplitude leads to a 6 dB phase noise improvement; however, the phase noise is slightly decreased in the proposed GS-Colpitts VCO due to flicker noise in $\mathrm{g_m}$-boosting transistors $\mathrm{M_{3,4}}$.

B. Upconversion of the Switching Transistor Flicker Noise in Region III

As previously explained, the $1/\mathrm{f}$ noise of the tail current source through the AM-to-FM conversion caused by the nonlinearity of the switching transistor capacitance is the dominant factor degrading the close-in phase noise in region II. However, the dominancy of this effect decreases as the switching transistors mostly stay in the triode region (region III) since the time-averaged effective capacitance changes slowly (see Fig. 8(a)). In addition, the AM-to-FM conversion can be negligible in region III due to the limited oscillation amplitude. Therefore, in region III, another effect becomes the dominant mechanism determining the close-in phase noise.

From Fig. 1, when current source transistor $\mathrm{M_0}$ is biased in the saturation region, $\mathrm{M_0}$ provides high impedance to the second harmonic at the common-source node. However, with an increase in the tail current, when a large output amplitude forces the current source transistor into the triode region, the output impedance of the current source at the common-source node of the switching pairs decreases. This leads to an increase in the second harmonic current at the tail [8]. The flicker noise of the switching transistor modulates the second harmonic current and mixes down to the fundamental frequency through communication of the switching transistors [$\mathrm{M_{1,2}}$ in Fig. 1(a)]. The second harmonic current modulated by the $1/f$ noise of the switching transistor flows into the lower impedance path (capacitor) of the LC-tank and changes the effective capacitance. This results in frequency modulation, which in turn leads to phase noise degradation [16]–[18]. Therefore, the flicker noise of the switching transistor becomes the main mechanism for the generation of phase noise in the voltage-limited region (Part III of Fig. 5). In the proposed $\mathrm{g_m}$-boosted GS-Colpitts VCO shown in Fig. 1(b), there are two differential pair transistors ($\mathrm{M_{1,2}}$ and $\mathrm{M_{3,4}}$). However, the flicker noise of the $\mathrm{g_m}$-boosting transistor $(\mathrm{M_{3,4}})$ is the dominant noise source of the phase noise degradation since the switching transistors $\mathrm{M_{1,2}}$ do not share a common-source node and the second harmonic component is filtered at the LC-tank.

The flicker noise current at the drain is proportional to the transconductance of the transistor. In the triode mode, the flicker noise current is a linear function of the drain-source voltage. Therefore, the flicker noise current becomes smaller as the transistor operates more deeply in the triode region (smaller drain-source voltage). As discussed previously, the close-in phase noise in region III is mainly caused by upconversion of the flicker noise from the $\mathrm{g_m}$-boosting transistor $(\mathrm{M_{3,4}})$ in the proposed GS-Colpitts VCO. For the given amount of output voltage swing that sends the transistors into the triode region, the $\mathrm{g_m}$-boosting transistors $(\mathrm{M_{3,4}})$ of the proposed VCO experience deeper triode mode operation due to the capacitive voltage division $(\mathrm{C_1/C_2})$ compared to the switching transistors in the conventional cross-coupled VCO. Therefore, the $\mathrm{g_m}$-booting transistors in the proposed VCO contribute a smaller amount of $1/f$ noise compared to the switching transistors in the conventional cross-coupled VCO [Fig. 1(a)]. Furthermore, the flicker noise contribution of $\mathrm{M_{3,4}}$ can be reduced by feedback capacitors $\mathrm{C_1}$ and $\mathrm{C_2}$ in the proposed GS-Colpitts VCO. Fig. 10 shows the noise model of the two VCOs when the same amount of noise current is injected into the *LC* tank. The noise current injected into the effective total capacitance is the same as that in the inductor, since the reactive power must be equal between L and C. Therefore, the effective capacitance variation from switching transistor flicker noise can be estimated through the noise current injected into the inductor. As can be seen in Fig. 10(b), the noise current $i_{n,L}$', which flows into the inductor, can be attenuated by decreasing $\mathrm{C_1}$ in the proposed VCO, compared to that $(i_{n,L})$ of the conventional VCO in Fig. 10(a). Therefore, as the same amount of flicker noise current $i_{n,1/f}$ is injected in the two VCOs, the frequency modulation effect by the switching transistor flicker noise can be reduced in the proposed GS-Colpitts VCO.

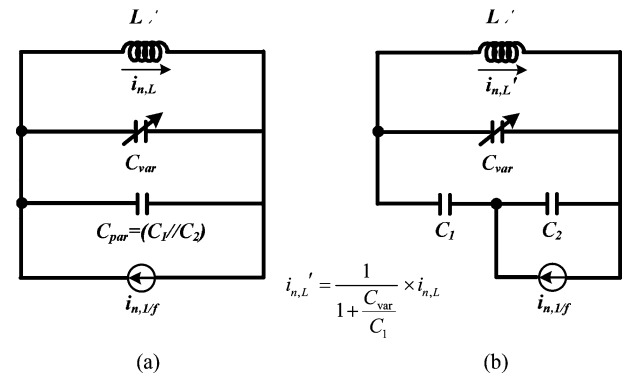

Fig. 10. Model of the flicker noise current for the (a) conventional cross-coupled and (b) $\mathrm{g_m}$-boosted differential GS-Colpitts VCOs.

This gives rise to improvement of the close-in phase noise in region III.

Fig. 11 presents a summary of the contributing noise sources to the phase noise of the two VCOs shown in Fig. 1 based on a simulation. In the conventional NMOS-only cross-coupled VCO, the close-in phase noise in region I ($\mathrm{I_{DD}} = 0.9$ mA, where the switching transistor operates between the cut-off and saturation modes) is mainly degraded by the flicker noise of the tail current source $(\mathrm{M_0})$ through the AM-to-FM conversion. In contrast, the contribution of the flicker noise of the switching transistor $(\mathrm{M_{1,2}})$ increases significantly in region III ($\mathrm{I_{DD}} =$ 9 mA, where the switching transistor operates in the triode mode and voltage limited region). However, in the proposed GS-Colpitts VCO, the phase noise degradation by the flicker noise of the switching transistors $(\mathrm{M_{1,2}}, \mathrm{M_{3,4}})$ contributes a smaller percent in total than that of the conventional VCO in region III.

Fig. 12 shows the simulated phase noise of the two VCOs using a resistor current source to verify the contribution of the flicker noise of the current source $(\mathrm{M_0})$ and switching $(\mathrm{M_{1,2}}, \mathrm{M_{3,4}})$ transistors. Compared to the phase noise characteristic with the current source transistor shown in Fig. 9, it can be seen in Fig. 12 that the flicker noise of the current source transistor is the dominant source, increasing the $1/f^3$ region of the phase noise in region II by the AM-to-FM conversion of the switching transistors, while the flicker noise of the switching transistor contributes significantly in the voltage limited region (region III) by the second harmonic modulation. The simulation results shown in Fig. 12 confirm the prediction that the flicker noise of the switching transistor $(\mathrm{M_{3,4}})$ in the proposed GS-Colpitts VCO can be attenuated by the feedback capacitors of $\mathrm{C_1}$ and $\mathrm{C_2}$ and by remaining in saturation mode for a short period of time, and thus the phase noise performance improves in region III.

As described in Sections II and III, adoption of the $\mathrm{g_m}$-boosting transistors $\mathrm{M_3}$ and $\mathrm{M_4}$ improves the start-up condition, increases the output swing (and therefore improves the phase noise), and suppresses the AM-to-FM conversion. The disadvantages of the $\mathrm{g_m}$-boosting transistors are additional thermal noise generation and the requirement of higher supply voltage, compared to the conventional cross-coupled VCO, due to additional transistor stacking.

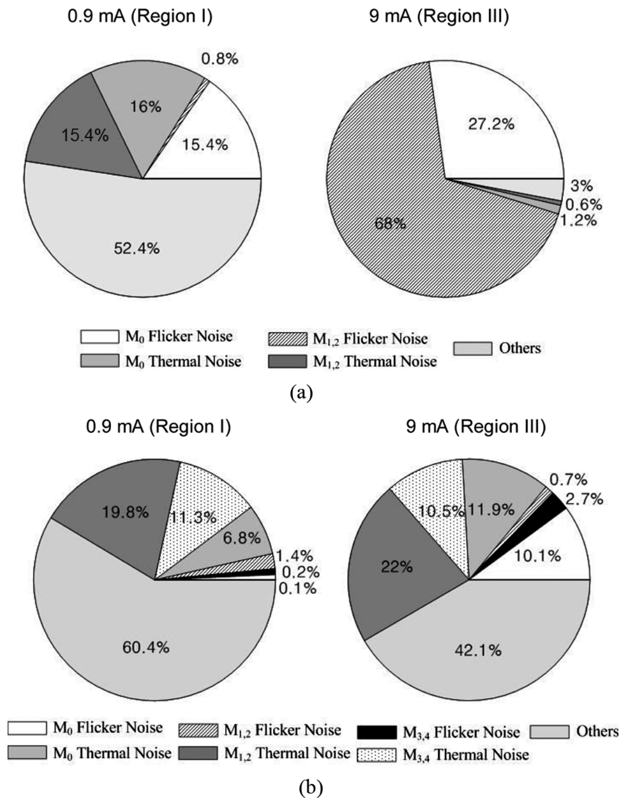

Fig. 11. Integrated phase noise contribution of each noise source ($10\,\mathrm{K} \sim 1\,\mathrm{M}$) in (a) conventional cross-coupled and (b) proposed GS-Colpitts VCO.

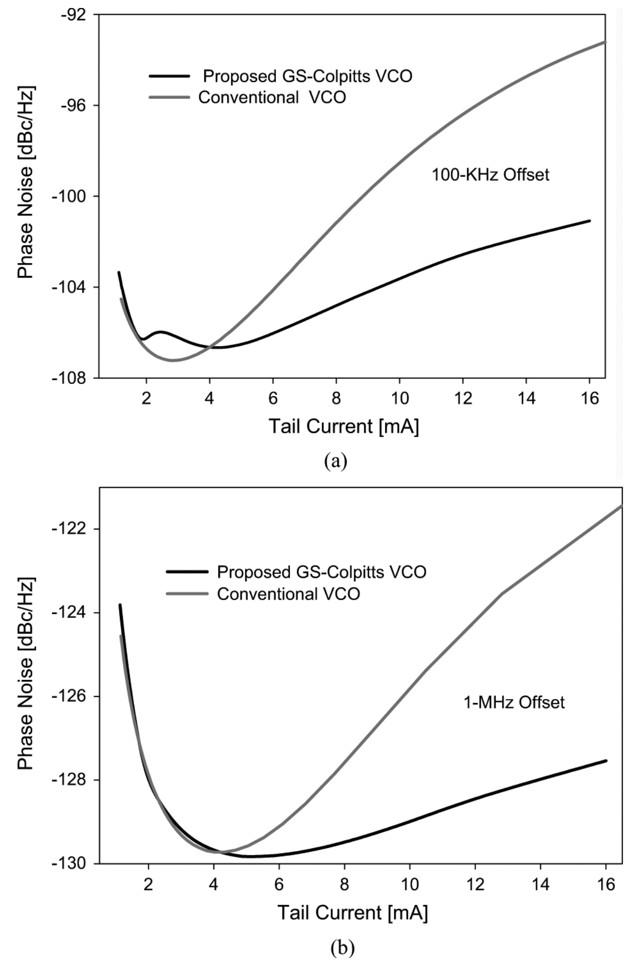

Fig. 12. Simulated phase noise at (a) 100 kHz and (b) 1 MHz offsets versus tail current in the conventional cross-coupled and g_m-boosted differential GS-Colpitts VCOs with a resistor current source.

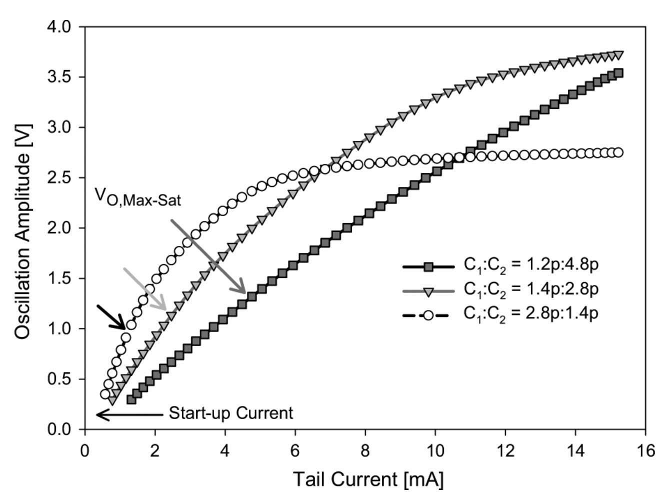

Fig. 13. Simulated output oscillation amplitude versus tail bias current by C_1/C_2 ratio in the proposed GS-Colpitts VCO.

C. Phase Noise Characteristic versus Feedback Capacitor Ratio

As previously discussed in Section II, the oscillation amplitude of the proposed g_m-boosted GS-Colpitts VCO increases with an increase in the C_1/C_2 ratio. Fig. 13 shows the simulated output amplitude versus tail current using three C_1/C_2 ratios, 0.25 (square), 0.5 (triangle down), and 2 (circle). In Fig. 13, the markers indicate the output oscillation amplitude at the maximum saturation operation point ($V_{O,Max-Sat}$) of the three C_1/C_2 ratios. As described above, the oscillation amplitude of the proposed g_m-boosted GS-Colpitts VCO increases with large $C_1/C_2 = 2$ ($C_1 : C_2 = 2.8p : 1.4p$ in Fig. 13) at the same bias current. As described in Section III-A, the oscillation amplitude at the maximum saturation mode operation ($V_{O,Max-Sat}$) is the same as the threshold voltage (V_{TH}) of the switching transistor in the proposed GS-Colpitts VCO. However, in practice, the proposed GS-Colpitts VCO with large $C_1/C_2 = 2$ becomes smaller than $V_{O,Max-Sat}$ relative to that of the small $C_1/C_2 = 0.25$, as shown in Fig. 13, since the drain-source voltage reaches $\upsilon_{DS} = 0$ earlier (less than V_{TH}). Therefore, $V_{O,Max-Sat}$ can be increased as the C_1/C_2 ratio decreases in the proposed GS-Colpitts VCO, even though the start-up current may increase.

To demonstrate the effect of the feedback capacitor ratio, the proposed GS-Colpitts VCO using three different C_1/C_2 feedback capacitor ratios of 0.25, 0.5, and 2 is designed to oscillate at the same frequency. Fig. 14 shows the simulated phase noise of the three VCO versions at offset frequencies of 100 kHz and 1 MHz. As can be seen in Fig. 14(a), in the saturation region (region I in Fig. 5), the proposed GS-Colpitts VCO shows better phase noise at $C_1/C_2 = 2$ (dashed-black) due to a larger output oscillation amplitude at the same tail current. However, the minimum close-in phase noise (-107 dBc/Hz) is achieved with

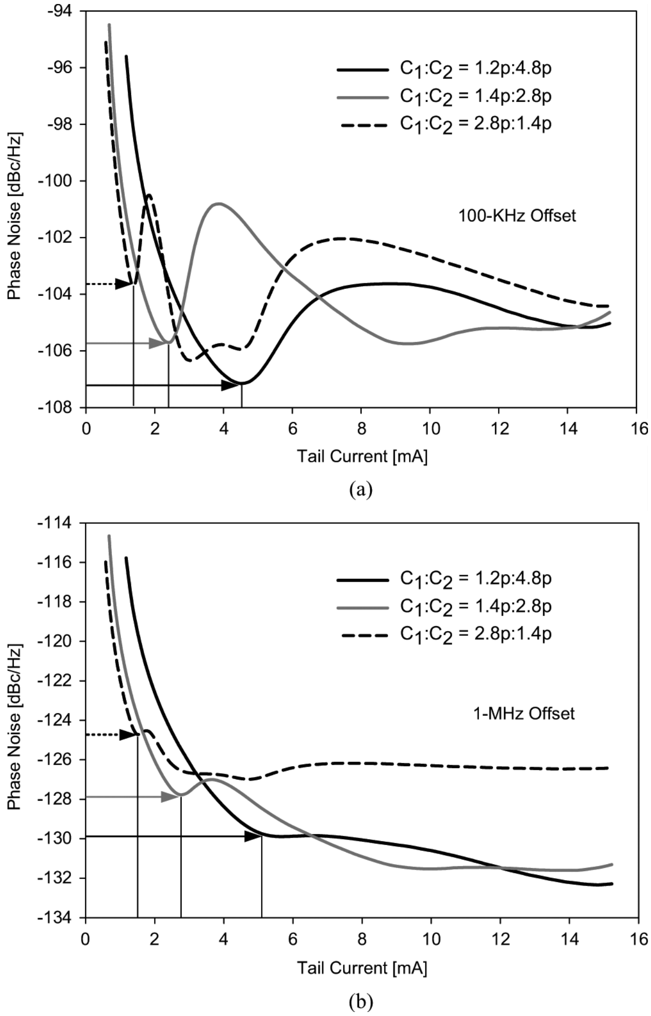

Fig. 14. Simulated phase noise at (a) 100 kHz and (b) 1 MHz offset for $C_1/C_2 = 0.25$ (solid-black), 0.5 (solid-gray), and 2 (dashed-black).

$C_1/C_2 = 0.25$ (solid-black) owing to the higher output oscillation amplitude ($V_{O,Max-Sat} = 1.24$ V) at the maximum saturation operation point (4.5 mA), which results from suppression of the AM-to-FM conversion by the switching transistors. In Fig. 12, the output amplitude in the large feedback capacitor ratio ($C_1/C_2 = 2$) reaches the voltage-limited region early (6 mA) and with a small voltage amount (2.5 V), since the high drain voltage of $M_{3,4}$ in Fig. 1(b) causes the current source transistor to enter the triode region at a lower tail current. However, the output oscillation amplitude with a small feedback capacitor ratio ($C_1/C_2 = 0.25$) still increases even at a large bias current (> 6 mA), since it operates under the current limited mode. As a result, the $1/f^2$ region (1 MHz offset) of the phase noise with $C_1/C_2 = 0.25$ (solid-black) shows better performance at a large bias current, as can be seen in Fig. 14(b). As mentioned in Section III-B, the effect of the second harmonic modulation, which is the main mechanism degrading the phase noise in the voltage-limited region, can be suppressed by decreasing the feedback capacitor ratio ($C_1/C_2 = 0.25$) in the proposed Colpitts VCO.

Most VCOs are designed to operate in region I of Fig. 5 to achieve an optimum figure-of-merit (FOM) and avoid unnecessary power dissipation. In the proposed g_m-boosted GS-Colpitts VCO, the feedback capacitor ratios have a trade-off relationship between a g_m-boosting effect and AM-to-FM conversion by the switching transistors. Therefore, in the proposed GS-Colpitts VCO, the capacitor feedback ratio can be selected by the priority of the specification; for example, when the phase noise requirement is critical and the power consumption characteristic is loose, the C_1/C_2 is designed at 0.25, and vice versa.

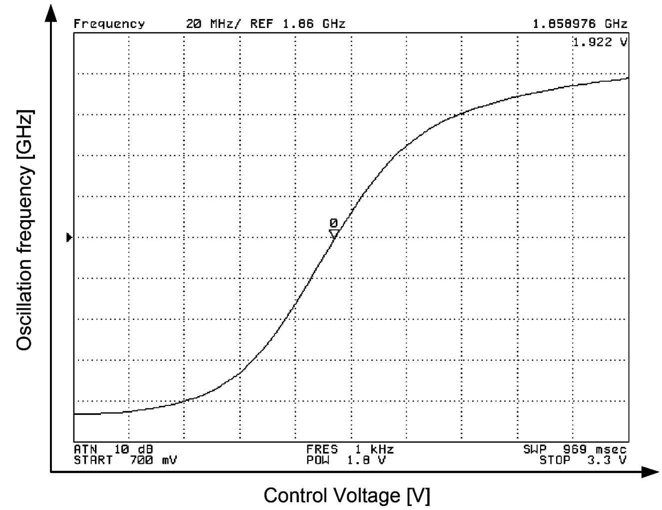

Fig. 15. Measured oscillation frequency versus the control voltage of the proposed GS-Colpitts VCO.

IV. Measurement Results

The proposed g_m-boosted differential Colpitts with $C_1/C_2 = 1$ and the conventional cross-coupled *LC*-VCO shown in Fig. 1 are implemented in a 0.18-μm CMOS technology. In the two VCOs, the same value as that of single MOS varactors is used for tuning. To deliver output power of the oscillator to a 50-Ω load, the open drain transistor M_{Buf} in Fig. 1 is used as a buffer. The phase noise of the implemented two VCOs is measured using a VCO/PLL signal analyzer. Fig. 15 shows the measured oscillation frequency versus the control voltage of the proposed GS-Colpitts VCO, showing an operating frequency range of 1.77 to 1.93 GHz over control voltage of 1.1 to 2.8-V. The conventional cross-coupled LC-VCO shows similar frequency behavior. Fig. 16 shows the measured oscillation frequency and frequency deviation versus tail current of the conventional [Fig. 16(a)] and proposed [Fig. 16(b)] VCOs. The tail bias current is swept by increasing the gate bias voltage of M_0. The oscillation frequency is measured at a center frequency of 1.86 GHz with 1.9-V control voltage, where the contribution of the varactor AM-to-FM conversion is negligible. As can be seen in Fig. 16, the measured oscillation frequency and frequency deviation curves of the two VCOs are in good agreement with the simulation results shown in Fig. 8: the maximum frequency deviation of the proposed GS-Colpitts VCO in Fig. 16(b) (114 MHz/V) is half that of the conventional NMOS-only cross-coupled VCO in Fig. 16(a)(-242 MHz/V). Fig. 17 shows the measured phase noise (100 kHz and 1 MHz offset) using a 1.8-V supply as a function of the tail bias current at a center frequency of 1.86 GHz. It can be seen that the overall

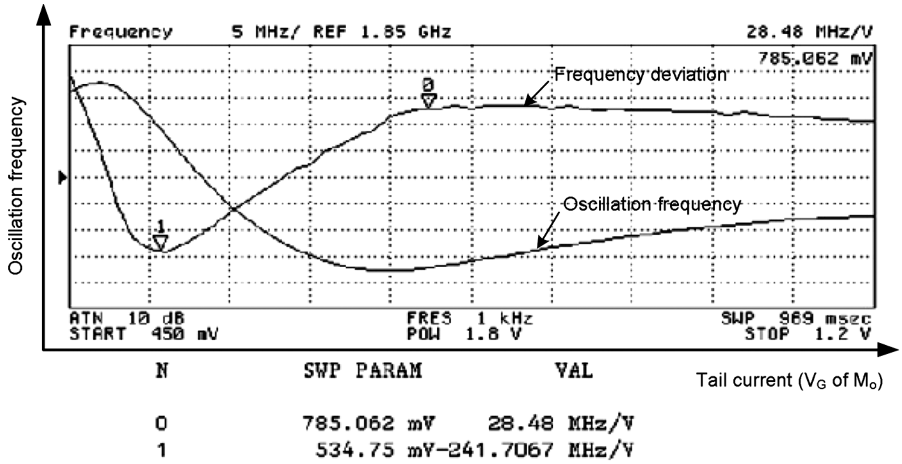

(a)

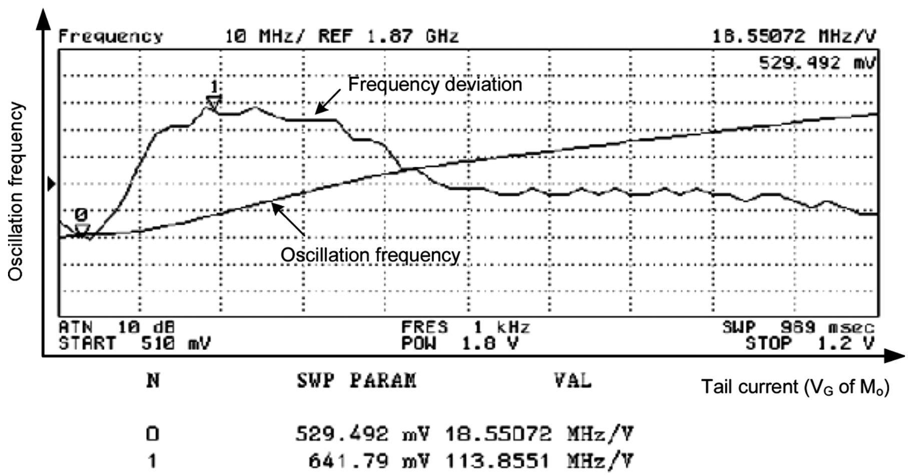

(b)

Fig. 16. Measured oscillation frequency and frequency deviation versus tail current for (a) the conventional cross-coupled and (b) g_m-boosted differential GS-Colpitts VCO.

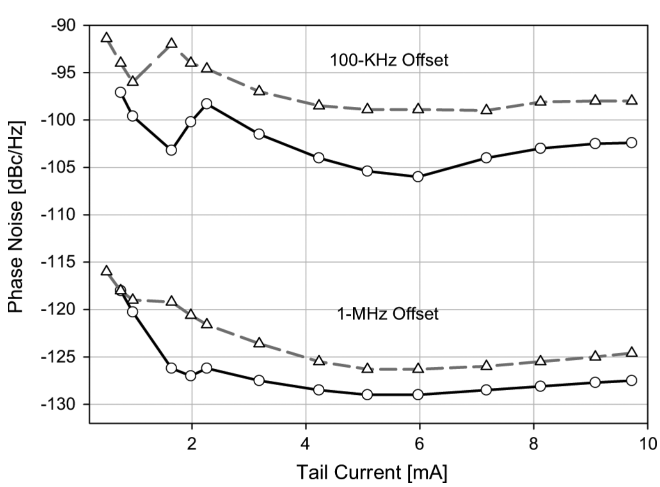

Fig. 17. Measured phase noise versus tail current of the proposed (circle) and conventional (triangle) VCOs at 1.86 GHz from a 1.8-V supply.

phase noise behavior shown in Fig. 17 is in good agreement with the theoretical predictions and simulation results shown in Fig. 9. Fig. 18 shows the measured FOM of the two VCOs at 100 kHz and 1 MHz offset with a 1.8-V supply. Compared to the conventional NMOS-only cross-coupled VCO (circle), the proposed GS-Colpitts VCO (triangle) shows a better FOM over the entire current range, as shown in Fig. 18. Fig. 19 shows the measured phase noise of the conventional NMOS-only cross-coupled and proposed g_m-boosted GS-Colpitts VCOs at 1.86 GHz while drawing 0.9 and 1.8 mA, respectively, from a 0.9-V supply. In Fig. 19, the tail current and supply voltage are adjusted in order to compare the phase noise performance of the two VCOs in their optimum operating conditions (the two VCOs operate in their lowest point of FOM, respectively). From Fig. 19, the measured phase noise of the proposed g_m-boosted differential Colpitts VCO is -105 and -128 dBc/Hz at 100 kHz and 1 MHz offsets, respectively, which correspond to a FOM of 191.2 dBc at a 1 MHz offset. Meanwhile, the measured phase noise of the conventional NMOS-only cross-coupled VCO is -94.5 and -119.5 dBc/Hz at 100 kHz and 1 MHz offsets, respectively, which correspond to a FOM of 186 dBc. As can be seen in Fig. 19, the proposed Colpitts VCO shows significant improvement in phase noise performance compared to the conventional cross-coupled VCO. Table I summarizes the performances of the proposed GS-Colpitts VCO compared to

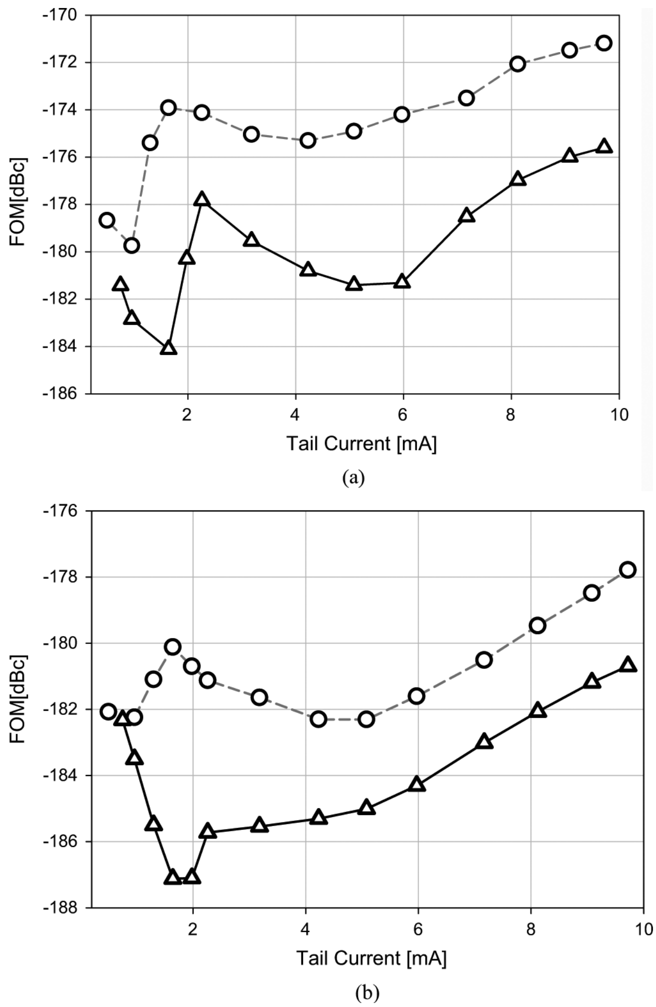

Fig. 18. Measured Figure of Merit (FOM) of Fig. 16 for conventional NMOS-only cross-coupled (circle) and g_m-boosted differential Colpitts (triangle) VCOs at (a) 100 kHz and (b) 1 MHz offset.

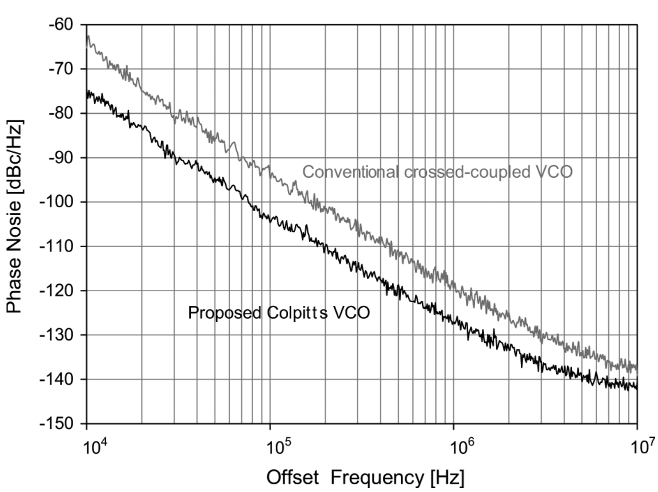

Fig. 19. Measured phase noise of the two VCOs at 1.86 GHz, with a current of 1.8 mA from a 0.9-V supply.

those of previously reported CMOS LC-VCOs using a current source transistor. The proposed g_m-boosted GS-Colpitts VCO shows good performance in all parameters. Fig. 20 shows a fabricated chip photograph of the two VCOs, where each VCO is $800 \times 680\ \mu\mathrm{m}^2$ in size excluding the pads.

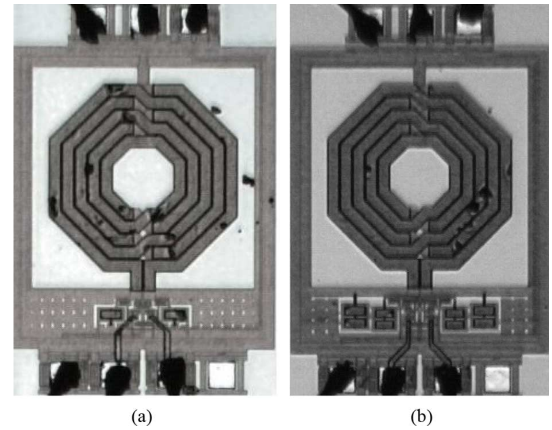

Fig. 20. Fabricated chip photograph of (a) the conventional cross-coupled differential and (b) proposed g_m-boosted Colpitts VCOs.

TABLE I
PERFORMANCE COMPARISON (VCOS USING CURRENT SOURCE TRANSISTOR)

VCO	Power [mW]	Supply [V]	Freq. [GHz]	Phase Noise [dBc/Hz]	FOM [dBc/Hz]	Tech. [μm]
[3]	10	2.5	1.8	-127@1MHz	-182.1	0.18
[4]	7.2	2	1.8	-128@1MHz	-184.5	0.18
[5]	1.4	1	4.9	-133@3MHz	-195.5	0.13
[9]	1.8	2.67	2	-103@100kHz	-182.3	0.18
[12]	16	2	2.9	-142@3MHz	-189	0.35
[12]	16	2	2.9	-138@3MHz	-184	0.35
This work	**1.6**	**0.9**	**1.86**	**-128@1MHz**	**-191.2**	**0.18**

V. DISCUSSION AND CONCLUSION

This work reports on a g_m-boosted differential GS-Colpitts VCO architecture that reduces the start-up bias current and increases the oscillation amplitude compared to a conventional Colpitts oscillator. An analysis of the oscillation amplitude and phase noise in the proposed GS-Colpitts is presented. The effect of the flicker noise of both the tail current and switching transistors is introduced and verified on the basis of the simulation results. Due to the feedback capacitor network in the proposed Colpitts oscillator, the maximum saturation mode of the operation point is delayed with an increase in output voltage swing, which helps to suppress the phase noise degradation by AM-to-FM conversion. The performance of the proposed g_m-boosted differential Colpitts VCO is demonstrated by simulations and measurements in comparison with the conventional Colpitts and conventional cross-coupled LC-VCO. The effect of the feedback capacitor ratio, C_1/C_2, in the proposed

$\mathrm{g_m}$-booted GS-Colpitts VCO is analyzed, and it is shown that the oscillation amplitude increases with increasing the ratio of $\mathrm{C_1/C_2}$, while the optimum phase noise $(\mathrm{FOM_{opt}})$ improves by decreasing the ratio of $\mathrm{C_1/C_2}$.

The proposed $\mathrm{g_m}$-boosted differential Colpitts VCO is implemented in a 0.18-μm CMOS for 1.77 to 1.93 GHz operation. The measured phase noise behavior at 1.86 GHz shows good close-in phase noise performance due to the suppression of AM-to-FM conversion by the switching transistors. At a center oscillation frequency of 1.86 GHz, the measured phase noises are -105 and -128 dBc/Hz (correspond to FOM of 191.2) at 100 kHz and 1 MHz, respectively, while dissipating 1.8 mA from a 0.9-V supply.

REFERENCES

[1] L. Hesen and E. Stikvoort, "An enhanced Colpitts UHF oscillator for TV tuners," in *Proc. European Solid-State Circuits Conf. (ESSCIRC)*, Sep. 1998, pp. 396–399.

[2] J. P. Hong and S. J. Lee, "Low phase noise G_m-boosted differential Colpitts VCO with suppressed AM-to-FM conversion," in *IEEE Radio Frequency Integrated Circuits (RFIC) Symp. Dig.*, Jun. 2009.

[3] R. Aparicio and A. Hajimiri, "A noise-shifting differential Colpitts VCO," *IEEE J. Solid-State Circuits*, vol. 37, no. 12, pp. 1728–1736, Dec. 2002.

[4] X. Li, S. Shekhar, and D. J. Allstot, "G_m-boosted common-gate LNA and differential Colpitts VCO/QVCO in 0.18-μm CMOS," *IEEE J. Solid-State Circuits*, vol. 40, no. 12, pp. 2609–2619, Dec. 2005.

[5] A. Mazzanti and P. Andreani, "Class-C harmonic CMOS VCOs with a general result on phase noise," *IEEE J. Solid-State Circuits*, vol. 43, no. 12, pp. 2716–2729, Dec. 2008.

[6] B. Jung and R. Harjani, "High-frequency LC VCO design using capacitive degeneration," *IEEE J. Solid-State Circuits*, vol. 39, no. 12, pp. 2359–2370, Dec. 2004.

[7] B. Soltanian and P. Kinget, "AM-FM conversion by the active devices in MOS LC-VCOs and its effect on the optimal amplitude," in *IEEE Radio Frequency Integrated Circuits (RFIC) Symp. Dig.*, Jun. 2006, pp. 11–13.

[8] E. Hegazi, H. Sjöland, and A. A. Abidi, "A filtering technique to lower LC oscillator phase noise," *IEEE J. Solid-State Circuits*, vol. 36, no. 12, pp. 1921–1930, Dec. 2001.

[9] D. J. Young, S. J. Mallin, and M. Cross, "2 Ghz CMOS voltage-controlled oscillator with optimal design of phase noise and power dissipation," in *IEEE Radio Frequency Integrated Circuits (RFIC) Symp. Dig.*, Jun. 2007, pp. 131–134.

[10] T. Song, S. Ko, D. Cho, H. Oh, C. Chung, and E. Yoon, "A 5 GHz transformer-coupled CMOS VCO using bias-level shifting technique," in *IEEE Radio Frequency Integrated Circuits (RFIC) Symp. Dig.*, Jun. 2004, pp. 127–130.

[11] Y. Wachi, T. Nagasaku, and H. Kondoh, "A 28 GHz low-phase-noise CMOS VCO using an amplitude-redistribution technique," in *IEEE Int. Solid-State Circuits Conf. (ISSCC) Dig. Tech. Papers*, Feb. 2008, pp. 482–483.

[12] P. Andreani, X. Wang, L. Vandi, and A. Frad, "A study of phase noise in Colpitts and LC-tank CMOS oscillators," *IEEE J. Solid-State Circuits*, vol. 40, no. 5, pp. 1107–1118, May 2005.

[13] B. Razavi, *Design of Analog CMOS Integrated Circuits*. New York, NY: McGraw-Hill, 2001.

[14] S. Levantino, C. Samori, A. Bonfanti, S. L. J. Gierkink, A. L. Lacaita, and V. Boccuzzi, "Frequency dependence on bias current in 5-GHz CMOS VCOs: Impact on tuning range and flicker noise upconversion," *IEEE J. Solid-State Circuits*, vol. 37, no. 8, pp. 1003–1011, Aug. 2002.

[15] E. Hegazi and A. A. Abidi, "Varactor characteristics, oscillator tuning curves, and AM-FM conversion," *IEEE J. Solid-State Circuits*, vol. 38, no. 6, pp. 1033–1039, Jun. 2003.

[16] A. Ismail and A. A. Abidi, "CMOS differential *LC* oscillator with suppressed up-converted flicker noise," in *IEEE Int. Solid-State Circuits Conf. (ISSCC) Dig. Tech. Papers*, Feb. 2003, pp. 482–483.

[17] J. J. Rael and A. A. Abidi, "Physical processes of phase noise in differential *LC* oscillator," in *Proc. IEEE Custom Integrated Circuits Conf. (CICC)*, Sep. 2000, pp. 569–571.

[18] H. N. Shanan and M. P. Kennedy, "A technique to reduce flicker noise up-conversion in CMOS *LC* voltage-controlled oscillators," in *Proc. European Solid-State Circuits Conf. (ESSCIRC)*, Sep. 2004, pp. 123–126.

[19] T. H. Lee, *The Design of CMOS Radio-Frequency Integrated Circuits*. Cambridge, U.K: Cambridge Univ. Press, 2004.

Jong-Phil Hong received the B.S. degree in electronic engineering from Korea Aerospace University, Seoul, Korea, in 2005 and the M.S. degree in engineering from the Information and Communications University, Korea, in 2007, and is currently working toward the Ph.D. degree in information and communications engineering at Korea Advanced Institute of Science and Technology (KAIST), Daejeon, Korea.

His main research interests include RF integrated circuits such as LNA, mixer, VCO and frequency synthesizer for wireless and wire-line communication systems using CMOS technology.

Sang-Gug Lee received the B.S. degree in electronic engineering from Kyungpook National University, Korea, in 1981, and the M.S. and Ph.D. degrees in electrical engineering at the University of Florida, Gainesville, in 1989 and 1992, respectively.

In 1992, he joined Harris Semiconductor, Melbourne, Florida, where he was engaged in silicon-based RFIC designs. From 1995 to 1998, he was with Handong University, Pohang, Korea, as an Assistant Professor in the School of Computer and Electrical Engineering. From 1998 to 2009, he was with the Information and Communications University, Daejeon, Korea, and become as a Professor. Since 2009, he has been with the Korea Advanced Institute of Science and Technology (KAIST), Daejeon, Korea, in the Department of Electrical Engineering as a Professor. His research interests include CMOS-based RF, analog, and mixed mode IC designs for various radio transceiver applications. Lately, his research interests are in low-power transceivers and extreme high-frequency (THz) circuit design based on CMOS technology, and display and energy-harvesting IC designs.